Available online at www.sciencedirect.com

ScienceDirect

Acta Materialia 84 (2015) 153–163

Acta MATERIALIA

www.elsevier.com/locate/actamat

Modification of eutectic Si in Al–Si alloys with Eu addition

J.H. Li,[a,*] X.D. Wang,[b] T.H. Ludwig,[c] Y. Tsunekawa,[d] L. Arnberg,[e] J.Z. Jiang[b,*] and P. Schumacher[a,f]

[a] *Institute of Casting Research, Montanuniversität Leoben, A-8700 Leoben, Austria*

[b] *International Center for New-Structured Materials (ICNSM), Laboratory of New-Structured Materials, State Key Laboratory of Silicon Materials, and Department of Materials Science and Engineering, Zhejiang University, Hangzhou 310027, China*

[c] *Hydro Aluminium AS, Årdal Metal Plant, N-6882 Øvre Årdal, Norway*

[d] *Toyota Technological Institute, Hisakata 2-12-1, Tempaku, Nagoya 468-8511, Japan*

[e] *Department of Materials Science and Engineering, Norwegian University of Science and Technology, N-7491 Trondheim, Norway*

[f] *Austrian Foundry Research Institute, Leoben A-8700, Austria*

Received 17 May 2014; revised 30 October 2014; accepted 31 October 2014

Abstract—Al–5 wt.% Si-based alloys with 0.05 wt.% Eu addition were produced by controlled sand-casting and melt-spinning, respectively. The modification of eutectic Si caused by 0.05 wt.% Eu addition was investigated by thermal analysis, differential scanning calorimetry and multi-scale microstructure characterization techniques. In the case of controlled sand-casting, 0.05 wt.% Eu addition was found to modify the eutectic Si into a fibrous morphology. Multiply twinned Si particles were observed within eutectic Si. Furthermore, the Al_2Si_2Eu phase was also observed both in the vicinity of eutectic Si and within eutectic Si, which was believed to hinder Si growth. In the case of melt-spun samples, nanometer-sized Al_2Si_2Eu phases were observed. However, after controlled cooling in a differential scanning calorimeter, multiply twinned Si particles were observed. The formation of multiply twinned Si particles was attributed to the adsorption of Eu atoms along the $\langle 1\,1\,2\rangle_{Si}$ growth direction of Si and at the intersection of two $\{1\,1\,1\}_{Si}$ facets. Twinning was observed in both fundamentally different casting processes: controlled sand-casting and melt-spinning. This is fully consistent with the well-known poisoning of the twin plane re-entrant edge and the impurity-induced twinning modification mechanisms.

Keywords: Al–Si alloy; Eu additions; Eutectic solidification; TEM; X-ray absorption spectroscopy

1. Introduction

The modification of the Si morphology from flake-like to fibrous form has been a long-standing topic in Al–Si alloys since 1921 [1], and is a key factor influencing the properties of Al–Si alloys. Modification is normally achieved by the addition of certain modifying elements with a favorable atomic size ratio (chemical modification) [2–20]. Two types of modifying elements have been reported. One type can modify the Si morphology from flake-like to fine fibrous, i.e. Na [1] and Sr [6–9]. The other type can only refine the eutectic Si, i.e. Yb [10] and Ca [11,12]. Both cases have been widely investigated. However, the exact modification mechanism that can be used to interpret these types of behavior for different elements remains unclear.

To date, it is generally accepted that the impurity-induced twinning (IIT) mechanism [2] and the twin plane re-entrant edge (TPRE) mechanism [3,4] as well as poisoning of the TPRE mechanism [5] are valid under certain conditions. The IIT mechanism postulates that the modifying elements (i.e. Sr and Na) are adsorbed on the growing $\{1\,1\,1\}_{Si}$ surfaces, producing frequent twinning. The TPRE mechanism proposes that Si growth occurs more readily at the re-entrant edge, while poisoning of the TPRE mechanism assumes that the modifying elements retard Si growth by selectively adsorbing at TPRE and thus deactivating the growth advantage of the TPRE mechanism. However, the IIT, TPRE and poisoning of TPRE mechanisms cannot be used to interpret all the observations accompanying modification. For example, the addition of Yb to hypoeutectic Al–Si alloys only refines, rather than modifies, the eutectic Si [10,14–16], even though Yb possesses a favorable atomic radius ratio ($r_{Yb}/r_{Si} = 1.646$) according to the IIT mechanism.

Among the rare-earth elements, it has been reported that only Eu can modify the eutectic Si to a fibrous morphology [13,14]. It appears that the behavior of Eu is similar to that of Sr and Na. However, there is still a lack of detailed investigations on the effects of Eu on the modification of eutectic Si under different solidification conditions (i.e. controlled sand-casting in Quik Cup or melt-spinning). In particular, the distribution of Eu atoms within eutectic Si (i.e. at the

* Corresponding authors. Tel.: +43 3842 402 3304; fax: +43 3842 402 3302 (J.H. Li). Tel.: +86 571 87952107; fax: +86 571 87951528 (J.Z. Jiang); e-mail addresses: jie-hua.li@hotmail.com; jiangjz@zju.edu.cn

http://dx.doi.org/10.1016/j.actamat.2014.10.064
1359-6462/

TPRE or at the intersection of Si facets and twins) and in the vicinity of eutectic Si has not been investigated in detail. Such information is of great importance to elucidate the well-known poisoning of the TPRE and IIT modification mechanisms. Here, it should be noted that IIT, TPRE and poisoning of the TPRE are described in terms of Si growth, while the nucleation of Si is also of great importance to elucidate the modification mechanism, as reported in the case of Na or Sr addition [6,17–19].

Crosley and Mondolfo [17] reported the poisoning effect of Na on AlP nucleation sites in P containing hypoeutectic Al–Si alloys. Na addition forces the nucleation of Si to larger undercooling. Similar results were also obtained by Ho and Cantor [18] in entrained droplet experiments. This was attributed to the formation of Na_3P compounds, which reduced the amount of the potent AlP phase. The poisoning effect of Sr on the AlP compound was reported by Cho et al. [19]. It was proposed that the intermetallic Al_2Si_2Sr compound consumed the AlP, thus reducing the number of nucleation sites for eutectic Si and, in consequence, also the nucleation frequency of macroscopic eutectic grains. In contrast, similarly to the formation of Na_3P compounds, the formation of Sr_3P_2 phase has also been suggested to reduce the amount of the AlP phase [6]. However, the effect of Eu on the nucleation of eutectic Si has not yet been reported, mainly because the inherent presence of impurities makes the investigation of nucleation notoriously difficult.

In this paper, the entrained droplet technique, which can be used to investigate isolated impurity effects on heterogeneous nucleation, was used to investigate the nucleation of eutectic Si in Al–5 wt.% Si-based alloy with 0.05 wt.% Eu addition. In order to compare the observations under different solidification conditions, the solidification behavior of the samples produced by controlled sand-casting and melt-spinning was investigated using thermal analysis (in Quik-Cup samples), differential scanning calorimetry (DSC) and multi-scale microstructure characterization techniques, with the aim of further elucidating the modification mechanism caused by different modifying elements.

2. Experimental methods

A series of Al–5 wt.% Si (hereafter referred to as Al–5Si) alloys (wt.%, used throughout the paper unless otherwise noted) with 0.05Eu (i.e. 0.05 wt.% Eu) addition were prepared using high-purity (HP) Al (5N, 99.998), HP Si chips (6N) and Eu pieces (2N8, 99.8). The addition of 0.05Eu was made using an Al–5Si–2Eu master alloy produced from HP Al (5N), HP Si chips (6N) and Eu pieces (2N8). The chemical concentration of Eu was determined by inductively coupled plasma atomic emission spectrometry (ICP-AES) apparatus. The P concentration was determined by glow-discharge mass-spectrometry (GD-MS) on a Finnigan ELEMENT GD instrument. The nominal compositions of other elements (Si and Al) are given in Table 1. It should be noted that the main focus of the present paper is on the Al–5Si alloy with 0.05Eu addition, because the required information of the binary Al–5Si alloy, as a reference, is already available from previous studies [6–8,10].

In the case of controlled sand-casting, the alloys were melted in an electric resistance furnace, and the temperature of the melt was kept constant at 720 °C. Each addition level was performed in a single batch. No degassing was performed prior to casting. At least two samples for each addition level were taken to perform thermal analysis using the Quik-Cup method. About 5 min after the addition of Al–5Si–2Eu master alloy, thermal analysis was performed to elucidate the thermal kinetics during solidification. The recalescence undercooling of the eutectic reaction (ΔT) was defined as the temperature difference between the growth temperature of the eutectic (T_G) and the minimum temperature of the eutectic (T_{min}).

Table 1. Measured compositions of Al–5Si-based alloy with 0.05Eu addition (wt.%).

Alloys	Elements			
	Si	Eu	P (ppm)	Al
Alloy 1	5.00	–	0.44	Balance
Alloy 2	5.00	0.05	0.44	Balance

Optical microscopy (OM), scanning electron microscopy (SEM), electron probe micro analysis (EPMA), time-of-flight secondary ion mass spectrometry (ToF-SIMS) and transmission electron microscopy (TEM) were employed to characterize the as-cast microstructure in Al–5Si alloy with 0.05Eu addition. Samples for OM, SEM, EPMA, ToF-SIMS and TEM observations were taken from the center parts at the vicinity of the thermal couple. The specimens for OM investigation were mechanically ground, polished and then etched using a mixture of 13 g boric acid, 35 g HF and 800 ml H_2O. The same samples used for OM investigation were further investigated using SEM and EPMA element mappings on a JEOL JXA-8500F equipped with wavelength dispersive X-ray spectrometers and ToF-SIMS (Ion-Tof GMbH). ToF-SIMS was operated in a pulsed dual beam mode where the sputtering ion sources were Cs^+ and O_2^+, and the analysis ion source Bi^+. The specimens for TEM investigation were mechanically ground, polished and dimpled to ~30 μm, and then ion-beam milled using a Gatan Precision Ion Polishing System (PIPS, Gatan model 691). TEM measurements were performed using a Philips CM12 microscope operated at 120 kV and an image-side Cs-corrected JEOL-2100F operated at 200 kV. The small beam diameter of the JEOL-2100F makes it possible to measure the composition of trace elements (i.e. Eu) along the $\langle 1\,1\,2\rangle_{Si}$ growth direction of Si and at the intersection of two $\{1\,1\,1\}_{Si}$ twins.

In the case of melt-spinning, the Al–5Si alloy with 0.05Eu addition (~15 g) were remelted under high-vacuum conditions and ejected onto a rotating copper wheel (20 m s^{-1}). A power compensated PerkinElmer PYRIS Diamond DSC instrument under an Ar atmosphere was used to measure the entrained droplet undercooling with constant heating from 400 °C to 600 °C, holding for 1 min at 600 °C, and subsequent cooling to 400 °C at a rate of 10 K min^{-1}. At least two DSC measurements (~8 mg) were performed. Ribbons for TEM observation in melt-spun condition and after DSC-controlled cooling were prepared using the same method as for bulk samples.

Both X-ray fluorescence (XRF) mapping and in situ X-ray diffraction (XRD) were performed using the 15U beamline with a Si drift diode detector at SSRF, Shanghai, to further elucidate the distribution of Eu atoms within eutectic Si and in the vicinity of eutectic Si in melt-spun Al–5Si–0.05Eu alloy. For comparison, Al_2Si_2Eu crystalline powder was also investigated as a reference. The applied beam size was ~2 × 3 μm^2, with an energy of 18 keV. In the case of XRF mapping, the scan pitch was

$100 \times 100\ \mu m^2$, and the step size 5 μm in each direction. For each point, the integration time was 2.5 s. In the case of micrometer-sized XRD measurements, each XRD pattern was collected for 0.5 s using a Mar165 CCD detector and was then integrated with the FIT2D program [20], with the aim of detecting the existence of minor crystalline phases by selecting different regions on the mapping images.

Furthermore, the X-ray absorption fine structure (XAFS) spectra of Eu L-III edge (6977 eV) were measured in the fluorescence mode at beamline 1W1B-XAFS of BSRF, Beijing, using a Germanium solid-state detector, which enables the detection of the fine structure information for elements with a low concentration. As a reference, Eu_2O_3 crystalline powder was also measured. Standard data analysis was conducted using the Ifeffit software package [21].

3. Results

3.1. Controlled sand-casting

3.1.1. Thermal analysis

Fig. 1 shows typical cooling curves taken from the Al–5Si alloy with 0.05Eu addition. The eutectic nucleation temperature (T_N), at which nucleation starts, the minimum temperature (T_{Min}), at which nucleation ends, and the growth temperature (T_G) are marked in Fig. 1a and b. Note that T_N is extracted from the corresponding derivative curve (dT/dt) (Fig. 1b). The measured nucleation undercooling of eutectic Si (i.e. 7.4 °C) is significantly reduced compared with the equilibrium eutectic temperature (577 °C). The higher nucleation undercooling is in contrast to a small or no undercooling in binary Al–5Si alloy [8]. This strongly indicates that 0.05Eu addition may remove or deplete the nucleation sites for eutectic Si (most likely AlP, in the form of AlP patches). However, it should be noted that the nucleation temperature (T_N) can be greatly affected by the nucleation conditions in the alloys. Even in the presence of ~0.44 ppm P (Table 1), a significant change in the nucleation undercooling was observed. In contrast, no significant change was observed for the minimum temperature (T_{Min}). However, the eutectic growth temperature (T_G) was displaced to a lower temperature (i.e. 574.2 °C), suggesting that Eu addition does hinder the Si growth significantly. This argument can be further supported by the following microstructure characterizations.

3.1.2. As-cast structure

Fig. 2 shows eutectic structures observed by optical microscopy (OM) compared with those at a low magnification. Addition of 0.05Eu results in a very good modification

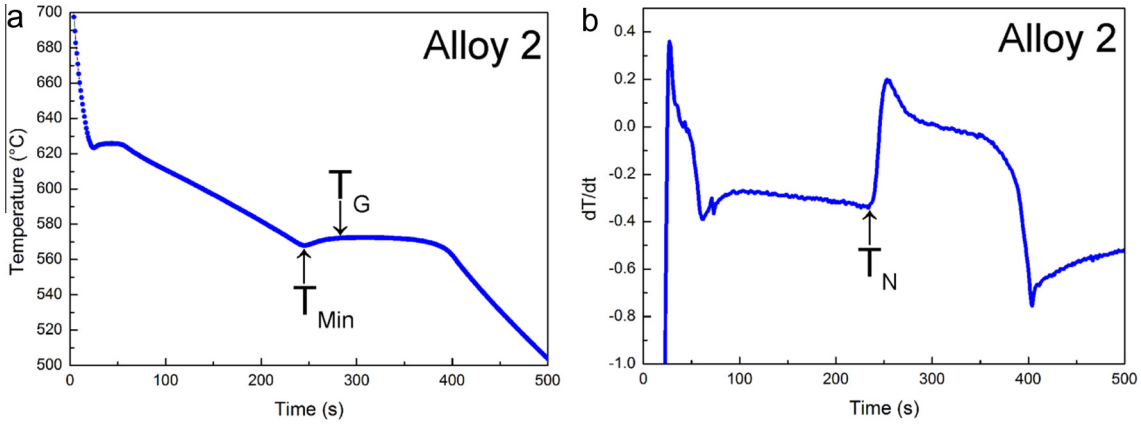

Fig. 1. Cooling curve and corresponding derivative curves (dT/dt) of Al–5Si alloy with 0.05Eu addition. The main points (T_N, T_{Min}, T_G) are also marked in (a) and (b), respectively. Note that T_N is extracted from the corresponding derivative curve (dT/dt) (b).

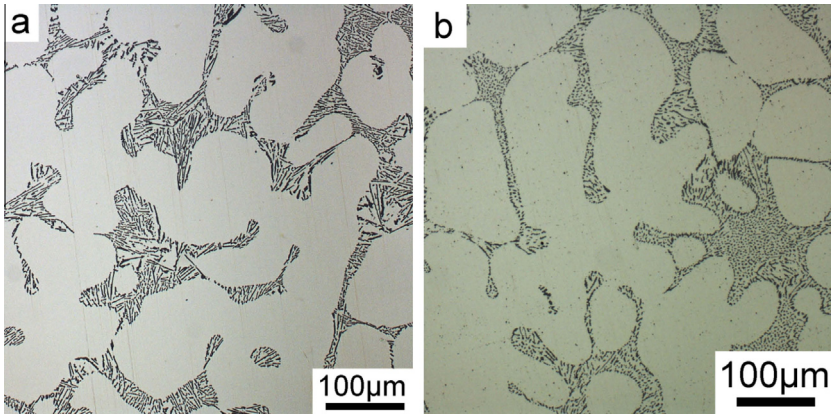

Fig. 2. Representative eutectic structure observed by OM at a low magnification taken from Al–5Si alloys (a) without and (b, c) with 0.05Eu addition. Note that the samples (a, b) were produced by controlled sand-casting (Quik-Cup).

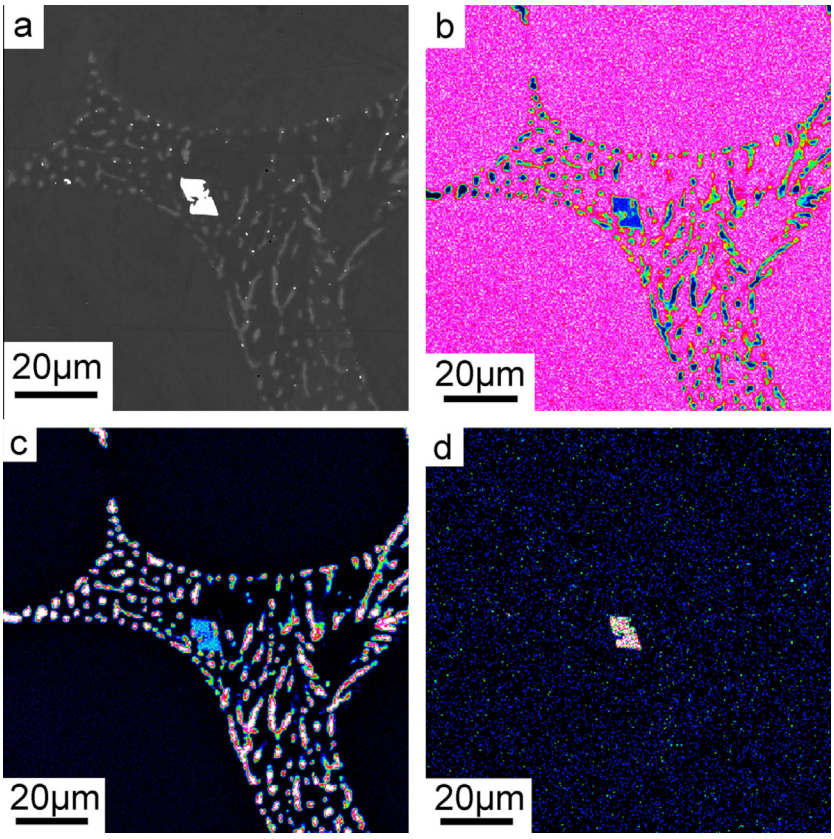

Fig. 3. EPMA mappings of eutectic Si and Al_2Si_2Eu phase in Al–5Si alloy with 0.05Eu addition: (a) SEM backscatter detection (BSD) image; (b) Al map; (c) Si map; (d) Eu map. Coarse Al_2Si_2Eu phase appears to be diamond-shaped or rhomboid in shape, and grows with defined facets. Note that the sample was produced by controlled sand-casting (Quik-Cup).

of the eutectic Si (Fig. 2b) compared with no Eu addition (Fig. 2a). The same samples used for OM investigation were further investigated using SEM and EPMA element mappings and ToF-SIMS. Similarly to Fig. 2b, well-modified eutectic Si was observed. In contrast to Fig. 2b, the coarse Al_2Si_2Eu phase was also observed within eutectic Si, as shown in Fig. 3a. Interestingly, the coarse Al_2Si_2Eu phase appears to be diamond-shaped or rhomboid in shape, and grows with defined facets. The coarse Al_2Si_2Eu phase can be expected to form as a pre-eutectic phase at sufficiently high Eu concentrations (i.e. 200 ppm Eu), similar to the Al_2Si_2Sr phase [7,8].

In addition to the coarse Al_2Si_2Eu phase, small Eu-rich particles are also observed in the vicinity of eutectic Si in Fig. 3. The small Eu-rich particles can be seen more clearly in Fig. 4 at a higher magnification. The small Eu-rich particles are marked with round white circles in Fig. 4d. This type of Eu-rich particle is believed to nucleate and grow ahead of Si within the segregation field of segregated elements (Al, Si).

The formation of Eu-rich clusters can be further supported using ToF-SIMS maps, as marked with round white circles in Fig. 5 with increasing magnifications from (a)–(c) to (d)–(f) and (g)–(i). The size of Eu-rich clusters is ~2 μm. Similarly to the report in Ref. [14], using the X-ray fluorescence (μ-XRF) technique, Eu was found to segregate strongly to the eutectic Si phase. No significant enrichment of Eu in the primary Al and eutectic Al was observed, which can be seen clearly in Fig. 5g–i. However, the atomic structures, i.e. nanometer-scale Eu-rich cluster or intermetallic within eutectic Si, cannot be investigated by ToF-SIMS, because of its limited resolution. The formation of Eu-rich clusters in the vicinity of eutectic Si can be related to the depression of the growth in Si by poisoning of the TPRE or IIT mechanism, which is consistent with the reduced eutectic growth temperature (T_G) during thermal analysis (Section 3.1.1).

3.1.3. TEM observation

Fig. 6a and b shows two Si particles along the grain boundary in Al–5Si alloy with 0.05Eu addition. One Si particle was tilted to the principal twinning orientation of Si ($\langle 1\,1\,0\rangle$) to observe Si twinning, as shown in Fig. 6b. The Si particle is multiply twinned, which can be seen clearly in Fig. 6c and d. Fig. 7 shows another Si particle along the grain boundary in Al–5Si alloy with 0.05Eu addition. Si twinning appears to occur along the $\langle 1\,1\,2\rangle_{Si}$ growth direction of Si, as marked with a dashed white line and a white arrow in Fig. 7a, indicating that eutectic Si grows along the TPRE. Furthermore, one Eu-rich particle was also observed within eutectic Si, as marked with a white arrow in Fig. 7b. This can be attributed to the solute entrapment during Si growth, caused by the formation of multiply Si twins [17]. Structural defects (i.e. Eu-rich clusters) appear to be present along the $\langle 1\,1\,2\rangle_{Si}$ growth direction of Si, suggesting poisoning of the TPRE, and at the intersection of two $\{1\,1\,1\}_{Si}$ twins, suggesting IIT, as shown in Fig. 7c and d, respectively. This observation is similar to the case of Sr and/or Na addition, underlining that the modification mechanism can be interpreted in a similar way.

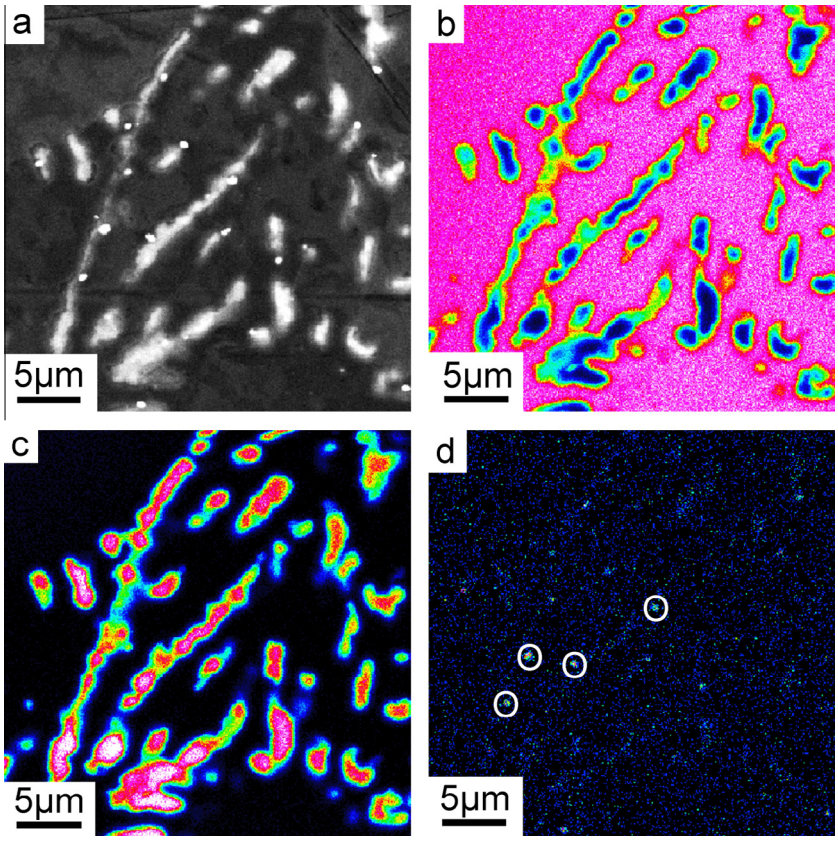

Fig. 4. EPMA mappings of eutectic Si and Al_2Si_2Eu phase in Al–5Si alloy with 0.05Eu addition: (a) SEM (BSD) image; (b) Al map; (c) Si map; (d) Eu map. Small Eu-rich particles were observed in the vicinity of eutectic Si, as marked with round white circles in (d). Note that the sample was produced by controlled sand-casting (Quik-Cup).

3.2. Melt-spun samples

3.2.1. DSC

Fig. 8 shows the DSC trace taken from Al–5Si with 0.05Eu addition at a constant rate of 10 K s^{-1}. Exotherm A corresponds to the solidification of the grain boundary eutectic [6]. Exotherm B is associated with the solidification of eutectic droplets embedded in the α-Al matrix. The undercooling of eutectic droplets can then be defined as the difference between the onset temperatures of exotherm A and exotherm B. As reported previously [6], the undercooling of the binary Al–5Si alloy is 20.5 °C (4 N Si), and 31 °C (5 N Si), respectively, depending on the impurity level of the Si used. A significant change in the undercooling of entrained eutectic droplets (51.9 °C) was observed with 0.05Eu addition. This strongly indicates that the presence of Eu may remove or deplete the nucleation sites for eutectic Si (most likely AlP, in the form of AlP patches), which is in an excellent agreement with the high nucleation undercooling achieved during thermal analysis (Section 3.1.1, Fig. 1). Another exotherm C was also observed in DSC traces at an onset temperature of 560.2 ± 0.5 °C. The exotherm C represents the formation of the Al_2Si_2Eu phase, which is also consistent with the microstructural observation (Fig. 3).

3.2.2. TEM observation

Fig. 9 shows TEM bright-field images of Eu-rich particles in melt-spun Al–5Si alloy with 0.05Eu addition. Higher cooling rates during melt-spinning result in a supersaturated Al–Si solid solution in which most Si is dissolved in the α-Al matrix. Therefore, no significant Si particle was observed in the melt-spun condition, compared with the case of controlled sand-casting. EDX analysis (Fig. 9d) and selected area diffraction pattern (SADP) (Fig. 9c) clearly indicate that the Eu-rich particle can be related to the Al_2Si_2Eu phase with a hexagonal close-packed structure ($a = 4.1839$ Å, $c = 7.2629$ Å).

After controlled cooling in DSC (from 600 °C to 400 °C with a constant rate of 10 K min^{-1}), multiply twinned Si particles were again observed, as shown in Fig. 10. Furthermore, an Eu-rich cluster (Al–Si–Eu) was also detected along the $\langle 1\,1\,2\rangle_{Si}$ growth direction of Si and at the intersection of two $\{1\,1\,1\}_{Si}$ twins (Fig. 10d). It is important to note that, at any other defect-free region, no significant Eu concentration can be measured. This result is fully consistent with the observation in controlled sand-casting (Figs. 6 and 7), and also in a good agreement with the XAFS spectra and analysis in Fig. 11.

3.2.3. Micrometer-sized XRD and XAFS investigation on melt-spun sample

In order to elucidate the Eu distribution within eutectic Si, Fig. 11a shows the micrometer-sized XRD pattern for the melt-spun Al–5Si–0.05Eu alloy. The presence of the Al_2Si_2Eu phase was clearly confirmed in the Eu-enriched regions together with Al and Si. However, it should be noted that, unlike TEM (Fig. 9), XRD results can be regarded as an average structural information within a micrometer-sized region. This suggests that the Al_2Si_2Eu

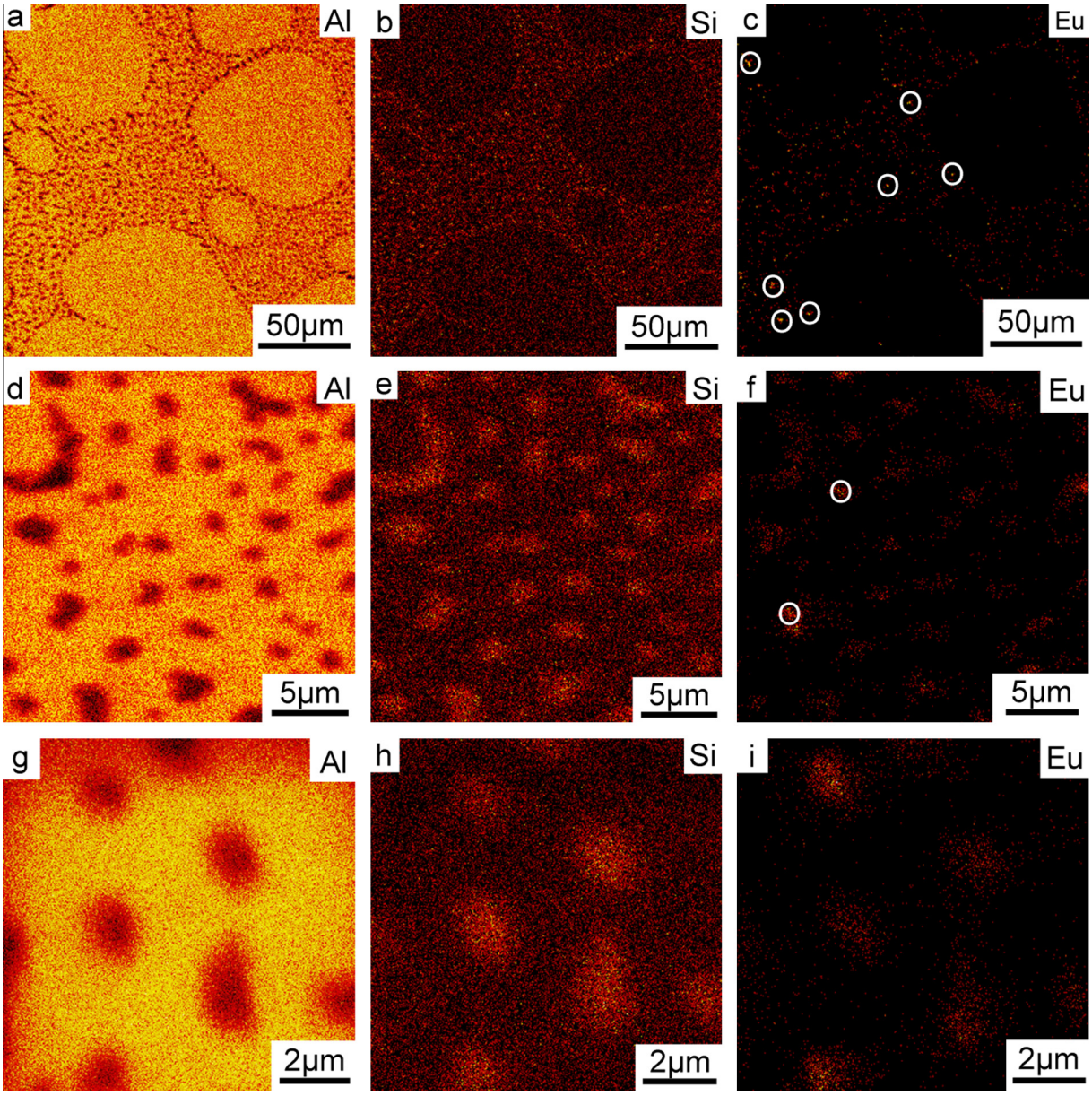

Fig. 5. ToF-SIMS maps taken from Al–5Si alloy with 0.05Eu addition: (a, d, g) Al map; (b, e, h) Si map; (c, f, i) Eu map with increasing magnifications. Small Eu-rich particles were marked with round white circles in (c) and (f), respectively. Note that the sample was produced by controlled sand-casting (Quik-Cup).

phase was indeed formed in Eu-enriched regions, even in the melt-spun sample.

In order to further elucidate the atomic environment of Eu atoms, XAFS spectra were measured. Fig. 11b shows the extended XAFS spectrum of the Eu L-III edge ($k^2\chi(k)$). For further analysis, Fig. 11c shows its Fourier transform. The amplitude of $|\chi(R)|$ in Fig. 11c gives the distribution of atoms around an Eu atom in real space. The first large peak in Fig. 11c is indicative of the signal from the first shell of atoms. Based on the Al_2Si_2Eu crystalline phase, a model was constructed to generate the FEFF paths for fitting the XAFS data. The fitting curves in the reciprocal and real spaces are also plotted in Fig. 11b and c, respectively. Good agreement with the experimental results was observed. Furthermore, the coordination numbers (CN), bond lengths (R), Debye–Waller factors (σ^2) and energy shift (ΔE) were determined and are listed in Table 2.

The CN of Eu–Si (CN = 4.88), Eu–Al (CN = 8.87), Eu–Eu (CN = 1.38) and Eu–Si (CN = 7.17) for which Si atoms are on the fourth shell in Al–5Si–0.05Eu alloy are different from that (CN = 6) in the Al_2Si_2Eu crystalline phase, especially for the Eu–Eu atoms, indicating that the Al_2Si_2Eu phase could be formed in Eu-enriched regions, but may be suspended in Eu-deficient regions, owing to a lack of sufficient Eu atoms, since Eu atoms are unevenly distributed, as shown in Fig. 5.

The bond length (R) is defined as the average distance between nuclei of two bonded atoms. When the bond length decreases, the bond energy increases, because the atoms are closer, and the forces of attraction are greater. In consequence, it would take more energy to break the bond. In the case of Al_2Si_2Eu phase, the bond length (3.081 Å) of Eu–Si is less than that of Eu–Al (3.568 Å), Eu–Eu (4.193 Å) and Eu–Si (5.101 Å) for which Si atoms

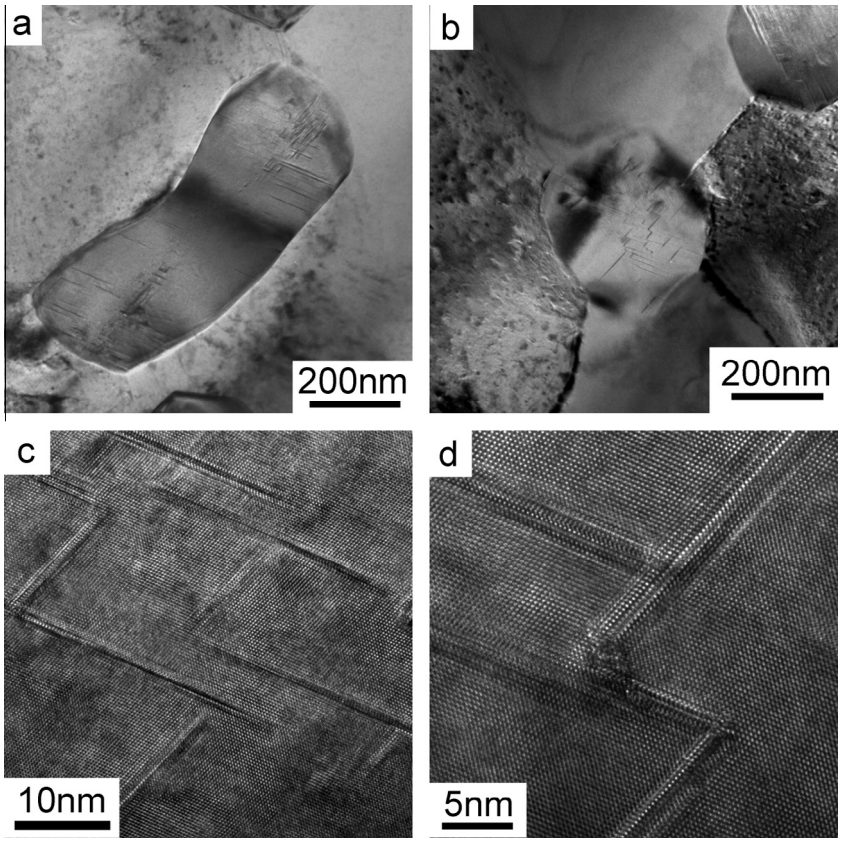

Fig. 6. (a, b) TEM bright-field images and (c, d) high-resolution TEM images of Si particles in Al–5Si alloy with 0.05Eu addition. Note that the sample was produced by controlled sand-casting (Quik-Cup).

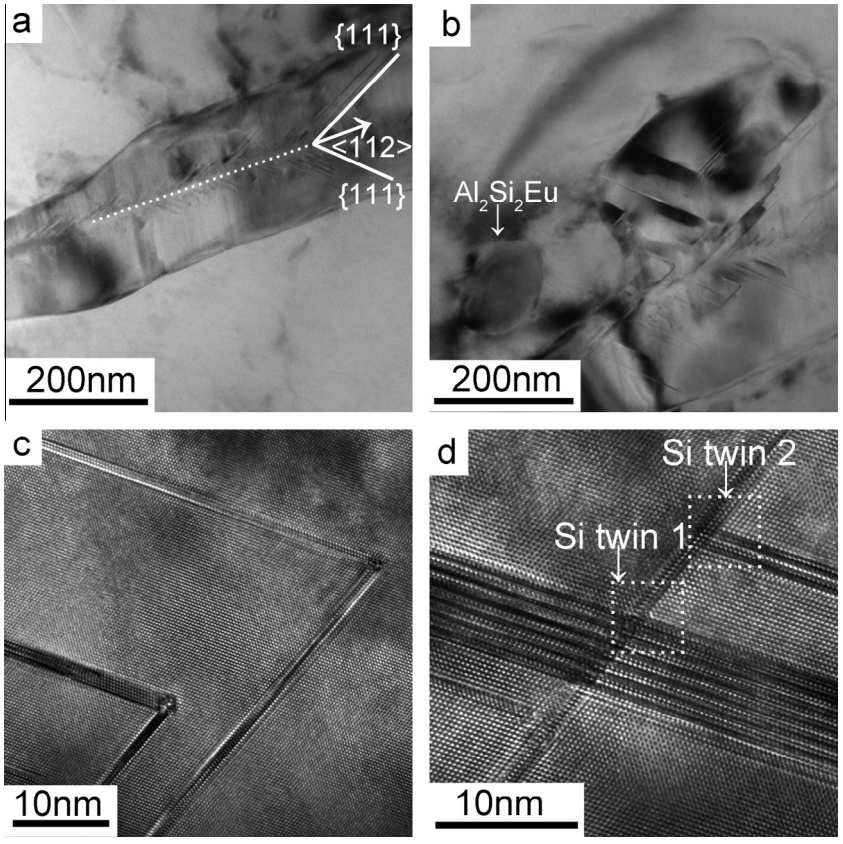

Fig. 7. (a, b) TEM bright-field images and (c, d) high-resolution TEM images of another Si particle in Al–5Si alloy with 0.05Eu addition. Note that the sample was produced by controlled sand-casting (Quik-Cup).

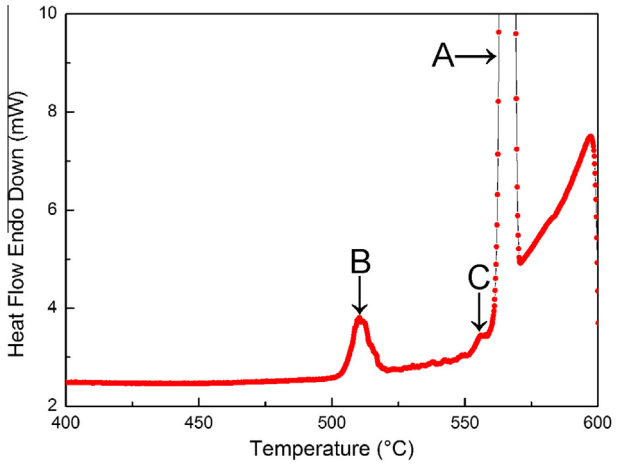

Fig. 8. DSC solidification traces after controlled cooling with a constant rate of 10 K min^{-1}, showing the exothermic reactions (A–C) for Al–5Si alloy with 0.05Eu addition. Note that the sample was produced by melt-spinning.

are on the fourth shell, respectively. Clearly, Eu is preferable to combine with Si, forming atom pairs or clusters. In the case of the Al–5Si–0.05Eu alloy, the bond length (3.12 Å) of Eu–Si is also less than that of Eu–Al (3.70 Å), Eu–Eu (4.23 Å) and Eu–Si (5.22 Å) for which Si atoms are on the fourth shell, showing that the bond length (R) between the center Eu atom and the atoms on the shells in the Al–5Si–0.05Eu alloy is almost identical to that in the Al_2Si_2Eu phase. This again provides strong evidence of the presence of the Al_2Si_2Eu phase.

Debye–Waller factors (σ^2) are defined as an indication of the relative vibrational motion of different parts of the structure. A lower value of the Debye–Waller factors (σ^2) means slower dynamics of the atom pairs. Thus, atoms pairs of Eu–Eu (0.001) and Eu–Si (0.009) have weaker vibrations than those of Eu–Al (0.037) and Eu–Si (0.015), for which Si atoms are on the fourth shell, indicating that an Eu atom has strong interactions with the nearest Si atoms.

4. Discussion

The addition of 0.05Eu to an Al–5Si alloy appears to have an important effect on the nucleation of eutectic Si. The measured undercooling of eutectic Si from thermal analysis (7.4 °C; Fig. 1) and the measured undercooling of entrained eutectic droplets from DSC traces (51.9 °C; Fig 8), clearly indicate that there is an interaction between Eu and P. However, it should be pointed out that the P content (0.44 ppm) in the present investigation is relatively low. In order to fully elucidate the interaction between Eu and P, a series of alloys with various P and Eu concentrations are required. Therefore, the effect of P on the nucleation of eutectic Si, which is mainly dependent on the P content, is not discussed further here. The following discussion will focus mainly on the roles of Eu during the growth of eutectic Si.

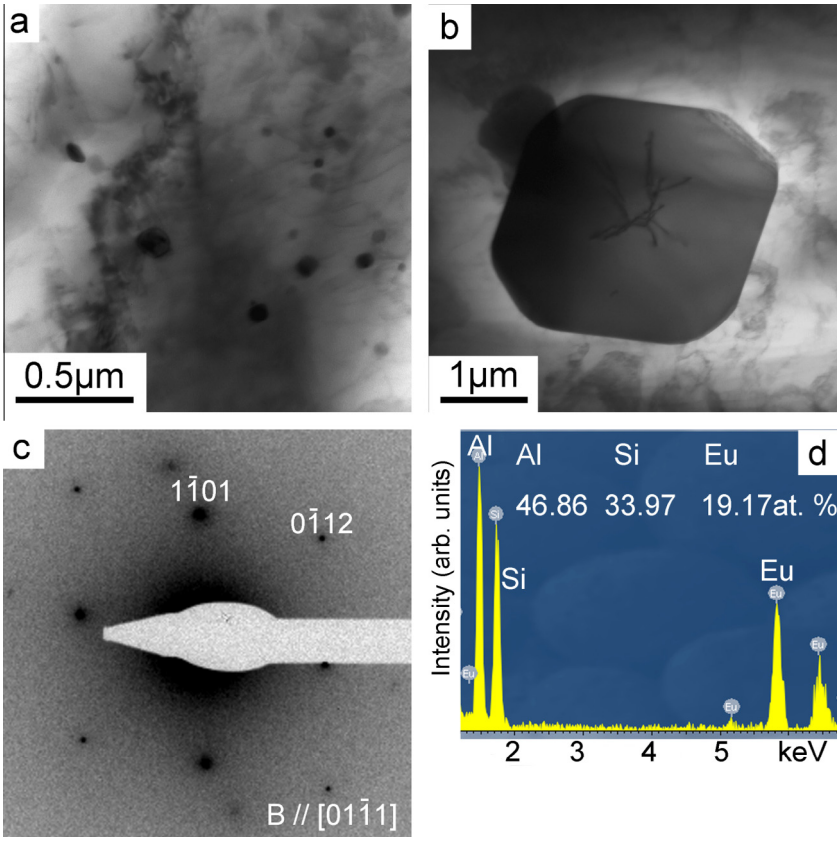

Fig. 9. (a, b) TEM bright-field images and (c) the corresponding SADP, (d) EDX analysis of Al_2Si_2Eu phase in Al–5Si alloy with 0.05Eu addition. Note that the sample was produced by melt-spinning.

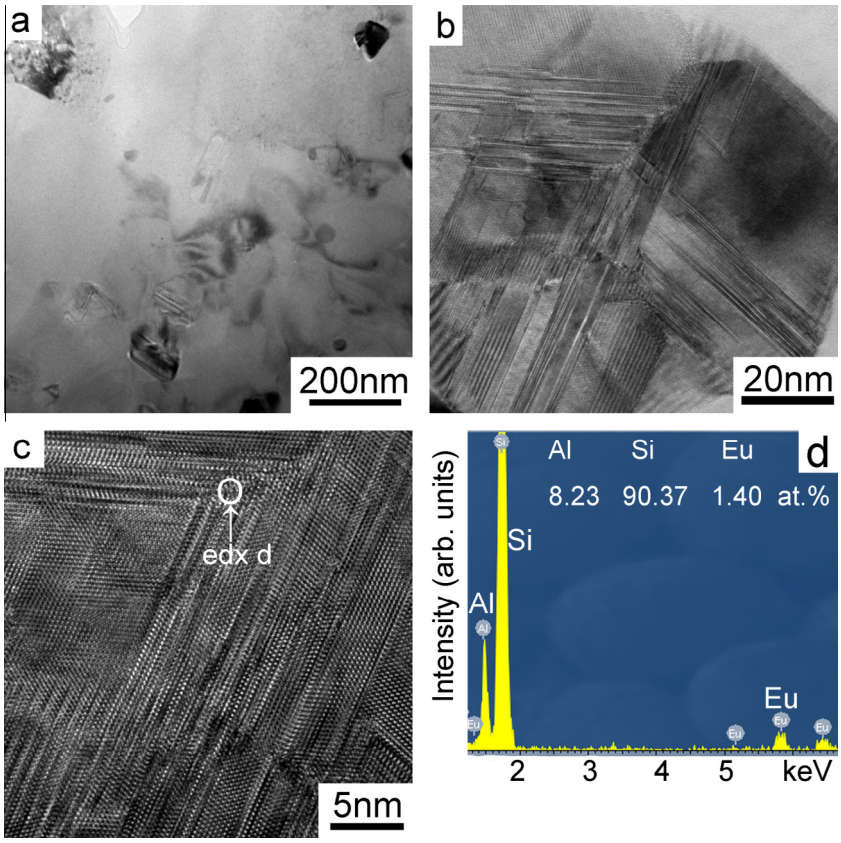

Fig. 10. (a) TEM bright-field image, (b, c) high-resolution TEM images, and (d) EDX analysis of the Si particle in Al–5Si alloy with 0.05Eu addition after DSC-controlled cooling from 600 °C to 400 °C at a rate of 10 K min^{-1}. Note that the sample was produced by melt-spinning.

The role of Eu during eutectic Si growth can be threefold. First, Eu contributes to the formation of the coarse Al_2Si_2Eu phase as a pre-eutectic phase before the eutectic reaction, which is very similar to the Al_2Si_2Sr [6–8], Al_2Si_2Yb [10] and Al_2Si_2Ca phases [11,12]. The coarse Al_2Si_2Eu phase was indeed observed in the cases of controlled sand-casting (Fig. 3). The pre-eutectic Al_2Si_2Eu phase can be due to the high Eu concentration (500 ppm), as an optical Eu concentration for modification is unknown. Further work is still required to optimize the Eu concentration required to obtain a fully fibrous eutectic Si. However, the coarse Al_2Si_2Eu phase is not believed to significantly affect the growth of eutectic Si.

Within eutectic Si, small Eu-rich clusters were proposed to be adsorbed along the $\langle 1\,1\,2\rangle_{Si}$ growth direction of Si and/or at the intersection of two $\{1\,1\,1\}_{Si}$ facets and twins in both cases of controlled sand-casting (Figs. 6 and 7) and controlled cooling in DSC of melt-spun ribbons (Fig. 10). The XAFS spectra and analysis (Fig. 11b, c and Table 2) indicate that Eu tends to bond preferably to Si. This bonding tendency is a strong argument for the adsorption of Eu atoms on $\{1\,1\,1\}_{Si}$ growth facets. For the successful adsorption of Eu atoms on $\{1\,1\,1\}_{Si}$ growth facets, these Eu atoms have to remain to be adsorbed sufficiently long so that they are not segregated out of Si, as Si has a very constrained solubility for Eu. The successful adsorption of Eu atoms on $\{1\,1\,1\}_{Si}$ growth facets forces the Si to grow around the Eu atoms. As the adsorption of Eu occurs preferably at naturally occurring TPRE, these TPRE can be blocked by the Eu atom and force the Si to grow after the Eu atom by adjunct $\{1\,1\,1\}_{Si}$ growth facets. Other studies [6,9,22] have shown that TPRE are decorated by elongated clusters enriched with the modifying element (i.e. Sr) and Al or by segregation lines formed by respective rows of single atoms during rapid quenching. This adsorption temporarily poisons the TPRE for Si growth so that other TRPE must be formed. In addition, there is a kinetic equilibrium of the adsorption of Eu atoms and their overgrowth by Si. The result is the decoration of TPRE by adsorbed Eu atoms.

For high rates of the adsorption of the Eu atoms, not only are TPRE poisoned, but also additional Eu atoms will be adsorbed on $\{1\,1\,1\}_{Si}$ facets. These sites are available for the IIT mechanism to create further facets and growth directions. IIT events ahead of the TRPE can result in an entrapment of the segregated Eu atoms pushed ahead of the growing Si and subsequent to the formation of single Eu-rich clusters by segregated Eu atoms. During continuous Si growth, the Al_2Si_2Eu particle (Fig. 7b) was formed within eutectic Si by solute adsorption and entrapment, which has been reported elsewhere in the case of addition of Sr and Na [22]. The adsorption of Eu atoms or the formation of Eu-rich clusters is believed to enhance the formation of $\{1\,1\,1\}_{Si}$ facets according to poisoning of the TPRE or IIT growth mechanism. A similar observation on the enrichment of Eu at the re-entrant edges of the eutectic Si has also been reported using the μ-XRF (X-ray fluorescence) technique [14]. Although further high-resolution characterization (i.e. atom probe tomography) on the distribution of Eu within eutectic Si is still required, the formation of Eu-rich clusters within eutectic Si can be regarded as the second role of Eu, which can be directly

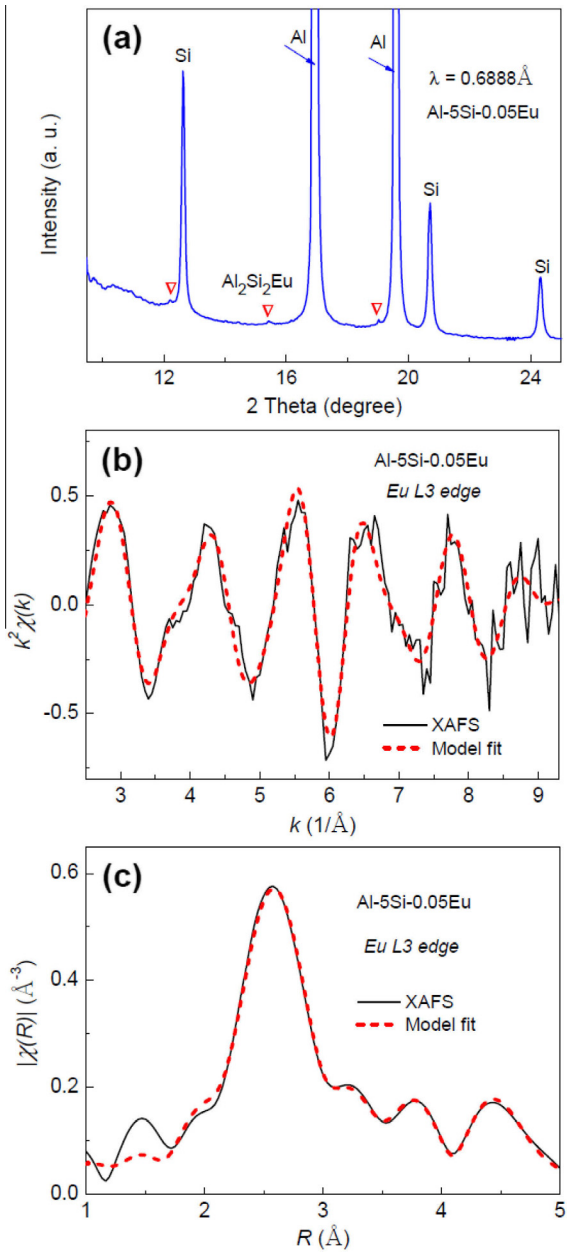

Fig. 11. (a) Microbeam XRD pattern for the Al–5Si alloy with 0.05Eu addition using the wavelength ($\lambda = 0.6888$ Å), demonstrating the presence of Al_2Si_2Eu phase in the Eu-enriched regions together with Al and Si. (b) XAFS spectrum at Eu L3 edge measured by a Germanium detector and fitted by a four-shell model centered by an Eu atom taken from Al_2Si_2Eu phase. (c) Amplitude of Fourier-transformed experimental and simulated XAFS spectra in real space. Note that the sample was produced by melt-spinning.

related to the poisoning of the TPRE and the active IIT growth mechanism.

The third role of Eu is to form the small Eu-rich particles (most likely Al_2Si_2Eu) in the vicinity of eutectic Si, as shown in Figs. 4 and 5. It should be noted here that, at high Eu concentrations, Eu that has not been adsorbed within eutectic Si will be segregated out of the Si during eutectic Si growth. Therefore, the Eu-rich particles in the vicinity of eutectic Si may form ahead of the growing Si crystal. This is different from the coarse Al_2Si_2Eu precipitating as a pre-eutectic phase (Fig. 3), and also from the Al_2Si_2Eu particle within eutectic Si (Fig. 7b).

Table 2. Comparison of the environment of Eu atoms in Al_2Si_2Eu phase and Al–5Si–0.05Eu alloy; the fitting ranges are $k = 2.5$–9.5 Å^{-1} and $R = 1.8$–5.3 Å.

Path	Al_2Si_2Eu phase		Al–5Si–0.05Eu alloy (XAFS)			
	CN	R (Å)	N	R (Å)	σ^2 (Å^2)	ΔE (eV)
Eu–Si	6	3.081	4.88 (2)	3.12 (6)	0.009 (6)	3.4 (4)
Eu–Al	6	3.568	8.87 (1)	3.70 (5)	0.037 (6)	7.9 (7)
Eu–Eu	6	4.193	1.38 (3)	4.23 (2)	0.001 (5)	8.4 (1)
Eu–Si[a]	6	5.101	7.17 (1)	5.22 (9)	0.015 (1)	1.9 (9)

[a] Si atoms are located on the fourth shell.

5. Conclusions

(1) The addition of 0.05Eu to Al–5Si alloys results in a very good modification of eutectic Si. A fibrous morphology involving Si twinning was achieved.
(2) A coarse Al_2Si_2Eu phase was observed as a pre-eutectic phase before the eutectic reaction. However, the coarse Al_2Si_2Eu phase is not believed to significantly affect the growth of eutectic Si.
(3) Small Eu-rich particles (most likely Al_2Si_2Eu phase) were observed in the vicinity of eutectic Si, which was believed to nucleate and grow ahead of Si within the segregation field of segregated elements (Al, Si).
(4) The Eu-rich clusters were observed along the $\langle 1\,1\,2\rangle_{Si}$ growth direction of Si and at the intersection of two $\{1\,1\,1\}_{Si}$ twins within eutectic Si, which provides strong experimental support for IIT and poisoning of the TPRE growth mechanisms, and can be related to the modification of eutectic Si from flake-like to fibrous morphology.
(5) The investigation highlights the importance of the adsorption of modifier during Si modification. However, only the modifier with a suitable atom size and a strong bonding with Si can be adsorbed along the $\langle 1\,1\,2\rangle_{Si}$ growth direction of Si and at the intersection of two $\{1\,1\,1\}_{Si}$ twins within eutectic Si. Therefore, not only the atom size, but also the bonding behavior with Si should be taken into consideration in order to achieve a good modification.

Acknowledgements

J.H. Li gratefully acknowledges the access to TEM at the Erich Schmid Institute of Materials Science of the Austrian Academy of Sciences. X.D. Wang and J.Z. Jiang gratefully acknowledge financial support from the National Key Basic Research Program of China (2012CB825700), National Natural Science Foundation of China (grant 51371157 and U1432105), and the Fundamental Research Funds for the Central Universities.

References

[1] A. Pacz, U.S Patent No. 1387900, 1921.
[2] Lu. Shu-Zu, A. Hellawell, Metall. Mater. Trans. A. 18 (1987) 1721–1733.
[3] R.S. Wanger, Acta Metall. 8 (1960) 57.
[4] R.D. Hamilton, R.G. Seidensticker, J. Appl. Phys. 31 (1960) 1165.
[5] M.G. Day, A. Hellawell, Proc. R. Soc. London A 305 (1968) 473–491.
[6] J.H. Li, M. Zarif, M. Albu, B. McKay, F. Hofer, P. Schumacher, Acta Mater. 72 (2014) 80–98.
[7] J.H. Li, M. Zarif, G. Dehm, P. Schumacher, Philos. Mag. 92 (2012) 3789–3805.
[8] M. Zarif, B. McKay, P. Schumacher, Metall. Mater. Trans. A 42 (2011) 1684–1691.
[9] M. Timpel, N. Wanderka, R. Schlesiger, T. Yamamoto, N. Lazarev, D. Isheim, et al., Acta Mater. 60 (2012) 3920–3928.
[10] J.H. Li, S. Suetsugu, Y. Tsunekawa, P. Schumacher, Metall. Mater. Trans. A 44 (2013) 669–681.
[11] T.H. Ludwig, E. Schonhovd Dæhlen, P. Schaffer, L. Arnberg, J. Alloys Compd. 586 (2014) 180–190.
[12] T.H. Ludwig, P. Schaffer, L. Arnberg, Metall. Mater. Trans. A 44 (2013) 3783–3796.
[13] K. Nogita, S.D. McDonald, A.K. Dahle, Mater. Trans. 45 (2004) 323–326.
[14] K. Nogita, H. Yasuda, M. Yoshiya, S.D. McDonald, K. Uesugi, A. Takeuchi, et al., J. Alloys Compd. 489 (2010) 415–420.
[15] K. Nogita, A. Knuutinen, S.D. McDonald, A.K. Dahle, J. Light Met. 1 (2001) 219–228.
[16] A. Knuutinen, K. Nogita, S.D. McDonald, A.K. Dahle, J. Light Met. 1 (2001) 229–240.
[17] P.B. Crosley, L.F. Mondolfo, Modern Castings 49 (1966) 63.
[18] C.R. Ho, B. Cantor, Acta Metall. Mater. 43 (1995) 3231–3246.
[19] Y.H. Cho, H.C. Lee, K.H. Oh, A.K. Dahle, Metall. Mater. Trans. A 10 (2008) 2435.
[20] A.P. Hammersley, S.O. Svensson, M. Hanfland, A.N. Fitch, D. Häusermann, High Pressure Res. 235 (1996) 14.
[21] M. Newville, J. Synchrotron Rad. 322 (2001) 8.
[22] J.H. Li, M. Albu, F. Hofer, P. Schumacher, Acta Mater. 83 (2015) 187–202.